

Comprehensive Symmetric-Hybrid ring design for pEDM experiment at below $10^{-29} e\cdot\text{cm}$

Zhanibek Omarov,^{1, 2} Selcuk Hacıömeroğlu,^{2, *} Valeri Lebedev,³ William Morse,⁴ Yannis K. Semertzidis,^{1, 2, *} A.J. Silenko,⁵ E.J. Stephenson,⁶ and more...

¹*Department of Physics KAIST Daejeon 34141 Republic of Korea*

²*Center for Axion and Precision Physics Research IBS Daejeon 34051 Republic of Korea*

³*Fermi National Accelerator Laboratory Batavia IL 60510 USA*

⁴*Brookhaven National Laboratory Upton New York 11973 USA*

⁵*Research Institute for Nuclear Problems Belarusian State University Minsk 220030 Belarus*

⁶*IUCF Indiana University Bloomington Indiana 47408 USA*

(Dated: September 2020)

To be rewritten later

I. INTRODUCTION

The possibility of the permanent electric dipole moments (EDMs) for elementary particles was initially proposed by Purcell and Ramsey [1] where the search for neutron EDM was used to investigate the parity-symmetry (P) violation. Later, it was also shown that non-zero EDMs separately violate time-reversal symmetry (T) by Landau [2].

Today's most advanced EDM experiments have set their limits on the parameter space: neutron EDM (nEDM) $< 3 \times 10^{-26} e\cdot\text{cm}$ [3], electron EDM (eEDM) $< 1.1 \times 10^{-29} e\cdot\text{cm}$ [4, 5], and mercury ^{199}Hg EDM $< 7.4 \times 10^{-30} e\cdot\text{cm}$ [6] which is equivalent to $2 \times 10^{-26} e\cdot\text{cm}$ for neutron and $5 \times 10^{-25} e\cdot\text{cm}$ for proton. Each of these experiments has different techniques, but all are similar as they require confined cold stationary particles. The Storage Ring Proton EDM not only has different systematics but also is the first dedicated EDM search experiment with relativistic particles. Having an experiment with a completely different design would be complementary to all the previous EDM experiments. It would also further expand the ground of storage ring high-precision experiments previously established by highly successful Muon ($g - 2$) experiments [7–10].

The storage ring proton EDM method targets $d_p = 10^{-29} e\cdot\text{cm}$ which is 3 orders of magnitude better than the current best neutron EDM limits. We also claim that this sensitivity is achievable with existing technology thanks to the significantly relaxed alignment requirements with the Symmetric-Hybrid ring design.

The most prominent systematic error source in the storage ring designs based on the all-electric ring [11] is the background radial magnetic field — B_x^{external} . All-electric ring designs variants are challenging due to immense average stray magnetic field requirements [12] — $B_x^{\text{external}} < 10^{-17} \text{ T}$.

To overcome such a challenging shielding requirement, the next iteration after the all-electric ring, the Hybrid

ring design [13] was developed. It has been a major accomplishment as for any B_x^{external} is naturally shielded by the magnetic focusing system. Hybrid ring design features strong alternating magnetic focusing with electric bending that still allows simultaneous Clockwise (CW) and Counter-Clockwise (CCW) beam storage.

In rings where the main vertical focusing is magnetic, the main systematic error source becomes the out-of-plane electric field. However, this systematic error cancels exactly for vertical dipole electric fields. It is the only lattice that accomplishes this cancellation and as such it represents a major breakthrough in the storage ring EDM field. The next level systematic error source is the fact that the average vertical velocity integrated over electric field sections might not be zero. This is a strict requirement for the case of radial polarization which has been relaxed by several orders of magnitude by making the lattice highly symmetric.

This work, the newest design iteration, the Symmetric-Hybrid ring relaxes requirements established by the Hybrid ring, provides comprehensive systematic error analysis, standardizes experimental techniques, and aims to be the conceptual foundational basis for the commissioning.

II. METHODS

A. Experimental Technique

The rest frame spin \vec{S} dynamics equation in presence of magnetic \vec{B} and electric \vec{E} fields is given as,

$$\frac{d\vec{S}}{dt} = \vec{\mu} \times \vec{B} + \vec{d} \times \vec{E}$$

where magnetic and electric dipole moments are defined as $\vec{\mu} = (ge/2m)\vec{S}$ and $\vec{d} = (\eta e/2mc)\vec{S}$ respectively.

However, for a particle with $\vec{\beta} = \vec{v}/c$ and $\vec{\beta} \cdot \vec{E} = 0$, $\vec{\beta} \cdot \vec{B} = 0$ the motion of the spin vector relative to the momentum can be more conveniently described by the BMT equation relative to a particle's momentum [14–

* Corresponding author

17],

$$\vec{\omega}_a = -\frac{e}{m} \left(G\vec{B} - \left(G - \frac{1}{\gamma^2 - 1} \right) \frac{\vec{\beta} \times \vec{E}}{c} + \frac{1}{\gamma} \left[\vec{B}_{\parallel} - \frac{1}{\beta^2} (\vec{\beta} \times \vec{E})_{\parallel} \right] \right) \quad (1)$$

$$\vec{\omega}_{\eta} = -\frac{\eta e}{2m} \left(\frac{\vec{E}}{c} + \vec{\beta} \times \vec{B} \right)$$

$$\vec{\omega}_{\text{total}} = \vec{\omega}_a + \vec{\omega}_{\eta}$$

$$\frac{d\vec{S}}{dt} = \omega_{\text{total}} \times \vec{S}, \quad (2)$$

with \parallel indicating horizontal projection of a vector.

It is readily seen that setting $\vec{B} = 0$ and choosing “magic momentum” such that $\gamma = \sqrt{1 + 1/G}$ leads to $\vec{\omega}_a = 0$ which is also known as frozen spin condition. In such an arrangement, the spin would precess in vertical direction due to the EDM contribution,

$$\omega_{\eta} \propto \eta E$$

linearly in the time scale of the fill $\omega_{\eta} \propto dS_y/dt$ [18, 19]. Further details about the proton electric dipole moment experiment could be found in [20, 21]

The Symmetric-Hybrid ring design used in this study consists of 24 FODO sections making up 800m in longitudinal length. Each FODO section comprises a pair of electric bending sections and a pair of magnetic quadrupoles. An illustration of a single FODO is given in Figure 1. The ring features complete 24-fold symmetry; hence, each FODO section is to be put right after the other without additional straight sections. A schematic of the ring is given in Figure 2. Dispersion and beta functions are given in Figure 4. More specs and details are given on Table I.

With such short straight sections, a vertical injection could be preferred.

It is important to note that the out-of-plane precession direction due to a genuine EDM signal would be opposite for counter rotating beams in the same storage ring. Namely ¹,

$$\left(\frac{dS_y}{dt} \right)_{\text{EDM}} = \frac{1}{2} \left(\frac{dS_y}{dt} \right)_{\text{CW}} - \frac{1}{2} \left(\frac{dS_y}{dt} \right)_{\text{CCW}}$$

vertical spin precession due to the EDM is the difference of vertical precessions of Clockwise (CW) and Counter-Clockwise (CCW) beams, with a factor of 1/2 that accounts for the effective doubling of the true EDM signal.

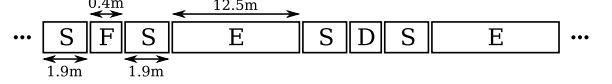


FIG. 1. Schematic view of a single FODO cell. The entire ring is composed by stacking this unit 24 times. Legend: F — Focusing quadrupole, D — Defocusing quadrupole, S — Straight section, E — Electric bending section.

In addition to having simultaneous storage of counter rotating beams, we can have another symmetrical flip — Polarity switch. It is the act of switching the direction of the currents in the magnetic quadrupoles. Quadrupoles being maximally current dominated makes it possible to phase shift the lattice beta functions by reversing direction of the currents in all of the magnetic quadrupoles. Then the EDM signal is given as,

$$\left(\frac{dS_y}{dt} \right)_{\text{EDM}} = \left[\frac{1}{4} \left(\frac{dS_y}{dt} \right)_{\text{CW}} - \frac{1}{4} \left(\frac{dS_y}{dt} \right)_{\text{CCW}} \right]_{\text{Polarity 1}} + \left[\frac{1}{4} \left(\frac{dS_y}{dt} \right)_{\text{CW}} - \frac{1}{4} \left(\frac{dS_y}{dt} \right)_{\text{CCW}} \right]_{\text{Polarity 2}} \quad (3)$$

B. High precision tracking

Runge-Kutta family integrator (5th order, adaptive step size [22]) was used in order to perform simulations throughout this work. Both beam and spin dynamics are fully tracked numerically. Particle beam dynamics are treated with perturbative expansion of the Lorentz equation around the reference orbit in Frenet-Serret coordinate system, with spin tracked via BMT equation. More details are given in Appendix A.

III. SYSTEMATIC ERROR SOURCES

The primary quantity of interest is the vertical spin precession rate dS_y/dt that lets us estimate the intrinsic dipole moment of the proton d_p . The target sensitivity of $d_p = 10^{-29} e \cdot \text{cm}$ that corresponds to the vertical spin precession rate is $dS_y/dt = 1 \text{ nrad/s}$. Thus, any non-EDM originating vertical spin precession rate at $dS_y/dt > 1 \text{ nrad/s}$ should be considered a potential systematic error.

Ideally, the EDM search is accomplished with positive helicity counter-rotating longitudinally polarized beams. Realistically, as little as $\approx 1/1000$ average radial spin component would be uncontrollable due to statistical limitations alone. Having such a mixing of longitudinal and

¹ y is vertical in lab frame

TABLE I. Ring and beam parameters for Symmetric Hybrid ring design

Quantity	Value
Bending Radius R_0	95.49 m
Electrode spacing	4 cm
Electrode height	20 cm
Deflector shape	cylindrical
Radial bending E -field	4.4 MV/m
Number of FODO sections	24
Straight section length	4.16 m
Quadrupole length	0.4 m
Quadrupole strength	± 0.21 T/m
Bending section length	12.5 m
Bending section circumference	600 m
Straight section circumference	200 m
Total circumference	800 m
Cyclotron frequency	224 kHz
Revolution time	4.46 μ s
Particles per bunch	2.5×10^8 (TBD)
Momentum spread, $(dp/p)_{\max}$	2×10^{-4}
Horizontal beta function, β_x^{\max}	64 m
Horizontal beta function, β_x^{\min}	35 m
Vertical beta function, β_y^{\max}	76 m
Vertical beta function, β_y^{\min}	41 m
Dispersion function D_x^{\max}	33 m
Dispersion function D_x^{\min}	24 m
Horizontal tune, Q_x	2.75
Vertical tune, Q_y	2.3
Slip factor, $\eta = \frac{dp}{p} / \frac{dt}{t}$	-0.28

radial spin directions might first seem as a major challenge. However, being able to control the mixing ratio between maximally longitudinal and maximally radial polarization is a powerful tool to clearly differentiate the systematic error sources into longitudinal and radial polarization originating types.

For instance, the beam placed in radial polarization with its vertical precession rate measured.²

Hence, any vertical spin growth inducer in radial polarization is a potential EDM systematic issue. The most prominent radial spin systematic is described in Section III A.

A. Vertical Velocity

Vertical velocity systematic originates from the proportional to

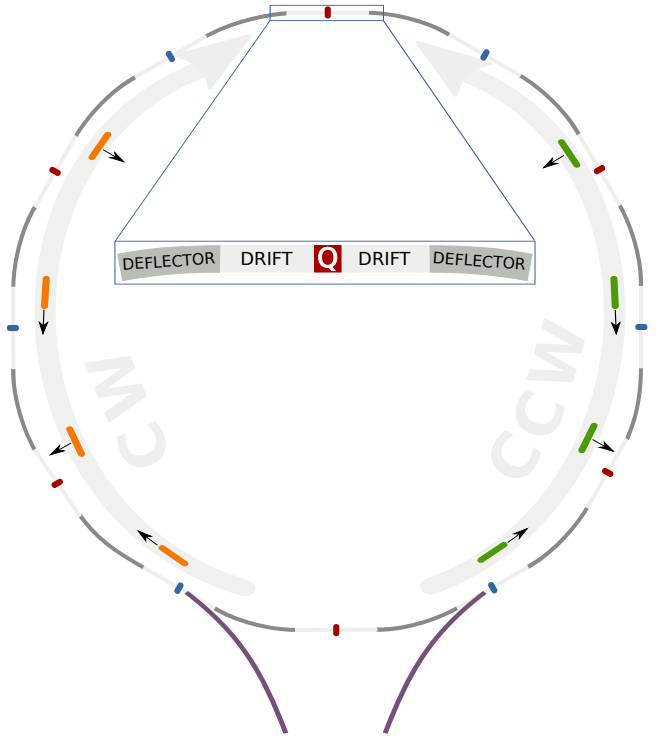


FIG. 2. Schematic top view of the symmetric ring. Both CW and CCW beams have longitudinally, radially, and vertically polarized bunches. Blue and red correspond to focusing and defocusing quads. Naturally, CW and CCW beams see opposite focusing effect from magnetic quads. The actual number of FODO sections is 24.

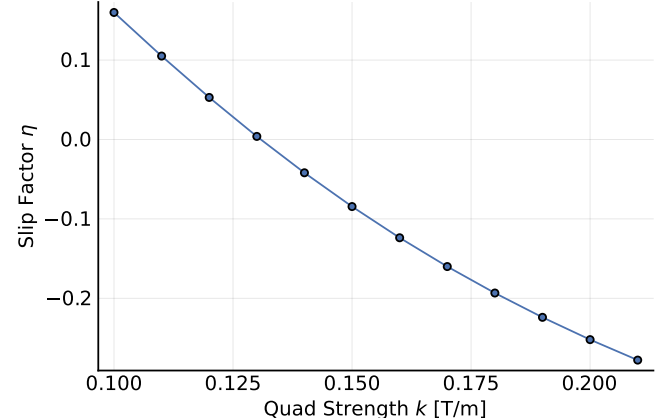


FIG. 3. The slip factor η is obtained from evaluating $\frac{dt}{t} = \eta \frac{dp}{p}$ per turn via numerical tracking.

$$\left(\vec{S} \times (\vec{\beta} \times \vec{E})_s \right)_y = S_x \beta_y E_x \quad (4)$$

² the polarization direction that does not manifest EDM induced vertical precession rate dS_y/dt due to the bending electric field E_x being along the spin direction

term in the BMT equation — Equation (2). Radial spin component S_x combined with vertical velocity β_y may create a vertical spin precession that would be indistin-

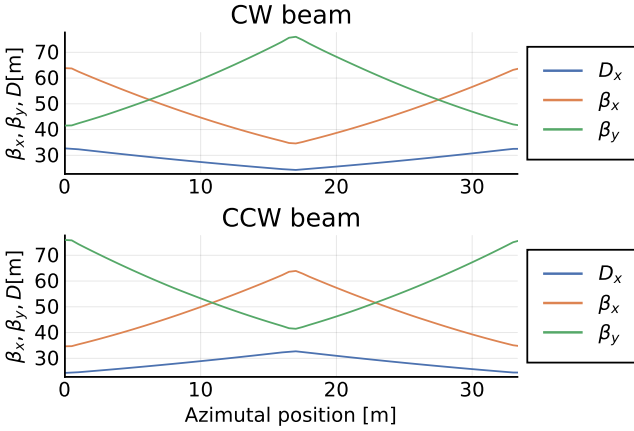


FIG. 4. Beta functions and dispersion along a single FODO section, 1/24 part of the storage ring (β letter within the text of the paper always refers to velocity).

guishable from EDM even with CW-CCW injection.

Despite $\langle \beta_y \rangle \equiv 0$, the velocity would be non-zero if averaged over the bending sections only (E_x field regions). Formally, we can only expect,

$$\langle \beta_y \rangle_{\text{straight}} + \langle \beta_y \rangle_{\text{bending}} \equiv 0,$$

but each of the $\langle \beta_y \rangle_{\text{straight}}$ and $\langle \beta_y \rangle_{\text{bending}}$ might not be zero individually. This leads to a possibility of

$$\langle \beta_y \cdot E_x \rangle \neq 0,$$

and,

$$dS_y/dt \propto \langle S_x \cdot \beta_y \cdot E_x \rangle \neq 0,$$

which is the essence of the effect.

This systematic is also known as vertical orbit corrugation or the “roller-coaster effect”. It is most prominent in the radial polarization case; thus its effect is at least few orders of magnitude less in longitudinal (EDM search) polarization. In order to isolate and understand this effect better, we put the beam in radial polarization and create vertical orbit corrugation by vertically misaligning one magnetic quadrupole at a time. A single vertically misaligned quad induces vertical imbalance that creates non-zero average vertical velocity.

This systematic is especially prominent in ring designs where the quadrupoles are not equivalent in misalignments with respect to each other. For example, the 4-fold symmetric hybrid ring design [13], (Figure 5), where misaligned quads are not equivalent (symmetric), shows clear islands of tolerance to vertical quad misalignments (Figure 6 (a)). This tells us that only the quads at the very symmetrical locations in the 4-fold symmetric ring are insensitive to the corresponding misalignments.

By making all the quads maximally symmetric (Fig-

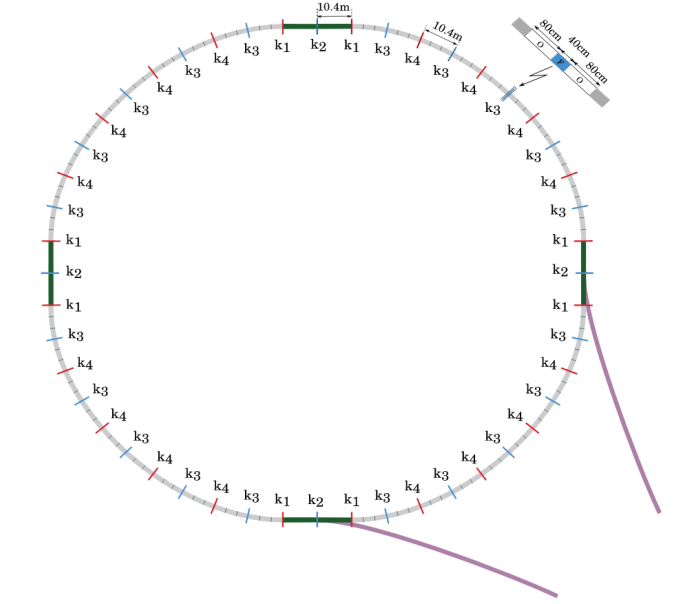


FIG. 5. 4-fold symmetric ring design, presence of the long straight sections reduce the number of symmetric points (adapted from [11])

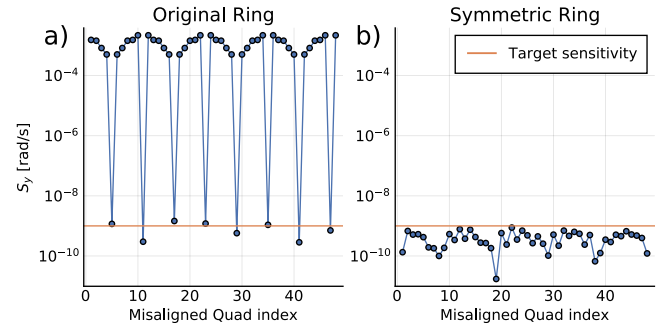


FIG. 6. *Radial polarization case.* Vertical spin precession rate vs. index of the 1 μm misaligned quad along the azimuth. The orange lines correspond to the target EDM sensitivity.

- (a) The original 4-fold symmetric ring design is used (Figure 5). Dips of the graph correspond to 1'30", 4'30", 7'30", 10'30" o'clock, and points in between shown in Figure 5.
- (b) The symmetric ring design is used (Figure 2). Notably the performance is many orders of magnitude better than 4-fold ring (a)

Irregularities of the low values are due to the inability to determine the exact precession rate from the simulation results. Hence, the points only show statistical upper limit of the possible vertical precession rate, actual rates could be lower.

ure 2) with respect to each other, we attempt to make all the quadrupoles equivalent and tolerant to vertical misalignments, Figure 6 (b). A vast improvement in the background vertical precession rate is achieved with symmetric ring design, therefore reducing the source of the systematic error by few orders of magnitude.

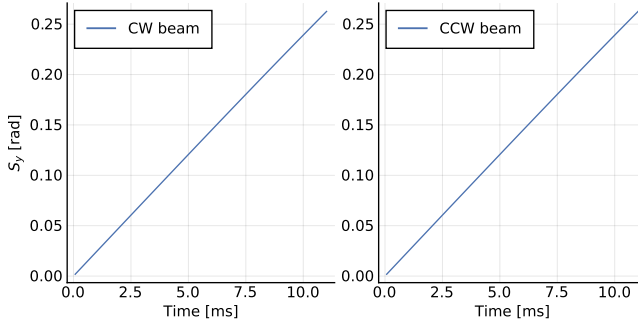


FIG. 7. *Longitudinal polarization case.* Vertical spin component vs. time. Opposite directions (CW and CCW) precess in the same direction (lab frame). EDM signal could be discerned by looking at the difference of the precessions.

B. Dipole E -field

The dipole E -field systematic originates from the

$$(\vec{\beta} \times \vec{E})_x = \beta_s \cdot E_y$$

term in Equation (2). Non-zero E_y could arise due to some tilt in the deflector plates. This creates an EDM-like signal for one of the counter rotating beams. However, a true EDM-signal would cause the vertical spin precession in opposite directions for CW and CCW beams. Hence, having CW and CCW beams is critical to combat this systematic, as the dipole E -field creates an opposite to the true EDM signal for each direction. Therefore, taking the difference of precession rates for CW and CCW beams gives us the true EDM signal, as the dipole E -field creates a discernible from EDM signal with CW and CCW beam storage. Formally,

$$\left(\frac{dS_y}{dt} \right)_{\text{EDM}} = \frac{1}{2} \left(\frac{dS_y}{dt} \right)_{\text{CW}} - \frac{1}{2} \left(\frac{dS_y}{dt} \right)_{\text{CCW}}.$$

The dipole E -field can happen due to some tilt in the bending plates. Let us assume a mechanical alignment of the tilts to $\sigma = 0.1$ mrad. Now, each bending section, being randomly tilted, contributes to the average non-zero dipole E -field in the storage ring. This creates vertical spin precession in CW and CCW beams Figure 7.

We can compensate for this non-EDM arising precession by applying opposite trim dipole field until no visible precession is seen in both directions – Figure 8. This trim field could be applied anywhere in the ring as long as it averages out the net E field to zero.

C. Quadrupole E -field

Storage rings having $\langle F_y \rangle = 0$ on the closed orbit by definition means that the quadrupoles compensate for any stray B_x^{external} and E_y^{external} – field directions primary

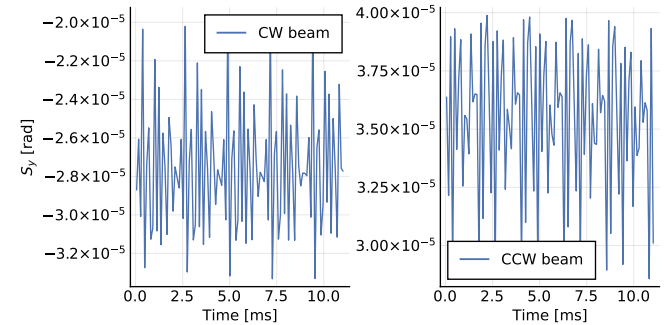


FIG. 8. *Longitudinal polarization case.* Vertical spin component vs. time. Opposite directions (CW and CCW) stop precessing if compensating trim field is setup at any position in the ring.

responsible for the equilibrium vertical position.

In the absence of vertical electric fields $E_y^{\text{external}} = 0$, any non-zero B_x^{external} would be compensated by a magnetic force coming from quadrupoles; therefore, it would on average result in $\langle B_x \rangle = 0$, which was confirmed numerically by simulations.

Putting it differently, in case of some B_x^{external} present it would be balanced by magnetic quadrupoles, and result in the average $\langle B_x \rangle = 0$. As in such a case, magnetic fields are balanced by magnetic fields; hence, there is no vertical spin precession due B_x .

However, in case $E_y^{\text{external}} \neq 0$, we can no longer guarantee $\langle B_x \rangle = 0$. We can only expect (to the first order, omitting “external” superscript),

$$\langle F_y \rangle = e \langle E_y - c \beta_s B_x \rangle = 0. \quad (5)$$

Equation (5) needs to be true throughout the ring, not just on average. This means that all the multipoles and harmonics of the E_y need to be accounted for. Fortunately, the most dominant multipole, dipole E_y and all harmonics are naturally accounted for with simultaneous CW-CCW storage.

Furthermore, it could be seen that symmetric with CW-CCW injection scheme multipoles, dipole, sextupole, decapole, etc., cannot induce EDM-like precession.

Next, quadrupole (and higher-order multiples of 4) E_y and its harmonics need to be dealt with. We need to note that the issue does not arise due to³ $E_{N=0,1,2,\dots}^{\text{quad}}$ directly, but its coupling with radial B_N field. That is, if some non-zero B_N is present then it would be partially compensated by electric focusing quadrupole — E_N^{quad} keeping Equation (5) correct. Since, the vertical spin precession occurs when electric force compensates magnetic force, being able to control one means we can control both.

³ x, y subscripts are dropped for clarity

The presence of E_N^{quad} can now be monitored by watching (dS_y/dt) . B_N should be adjusted along the ring azimuth until

$$\frac{\partial(dS_y/dt)}{\partial(B_N)} = 0$$

is reached, and this would cancel this systematic exactly. We argue that $\delta y \propto 1/(Q_y^2 - N^2)$ meaning that high order harmonics would not contribute as much, hence the cancellation is only needed for low values of N .

Transverse magnetic fields can also be accurately monitored by beam position monitors (BPM) using the K-modulation technique [23]. This technique basically relies on measurement of transverse oscillation amplitude of the beam(s) at a specific frequency, which is determined by modulating the quadrupoles. For the proposed ring, a 1 fT static radial magnetic field moves the beam vertically by 100 nm. Modulating the quad fields by 1% leads to a 1 nm oscillation amplitude, which induces roughly 1 fT magnetic field horizontally at a 2 cm away point on the horizontal plane. We are planning to employ a recently developed SQUID-based BPM, which has a $1 \text{ nm Hz}^{-1/2}$ sensitivity [24, 25]. Installing such a BPM at ten locations around the ring guarantees aT level transverse magnetic field for the first five multipoles.

Similarly, image charge, beam-to-beam, and etc. effects that may produce quadrupole electric field (or higher) component are treated the same way. The effect on the vertical spin precession rate does not depend on the origin of the electric field.

D. Geometrical Phase

Geometrical (Berry) Phase effect, as it is known in its most common definition, [26–28] is attributed to an extra acquired phase difference when a given system undergoes a cyclic adiabatic process.

In the context of storage ring EDM experiments, unwanted spin precession obtained due to non-commutativity of the successive rotations is referred to as Geometrical Phase. The spin precession is proportional to the product of successive rotation amplitudes.

We verify the product dependence, by linearly increasing the amplitude of successive rotations in the x, y plane. In this case, there are rotations in 2-d the plane, hence we must obtain a square dependence. This is accomplished by misaligning all magnetic quadrupoles by σ (both x, y directions) and keep increasing σ while observing the growth of the unwanted vertical precession rate. We place a single CW beam in longitudinal polarization and observe its spin precession rate against σ — Figure 9. Significant cancellation is achieved by incorporating both CW and CCW beams [29] with reversed magnetic quadrupole polarities.

Geometrical Phase could be produced due to misaligned magnetic quadrupoles, tilted misaligned electric

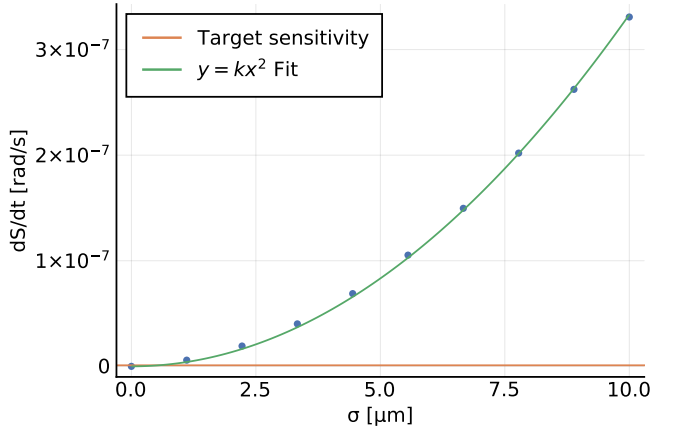


FIG. 9. *Longitudinal polarization case, CW beam only.* Vertical spin precession rate vs σ quadrupole misalignments. $\sigma = 1 \mu\text{m}$ is alignment is required with a single CW beam. Additional cancellation is achieved by incorporating polarity switches with CW and CCW beams, which vastly relaxes this requirement.

deflectors, or any other ring corrugation sources. Utilizing numerical tracking, we find that the EDM-like vertical spin precession caused due to Geometrical Phase is insignificant in case the orbit planarity is $\pm 50 \mu\text{m}$ with CW-CCW beam separation of $\pm 5 \mu\text{m}$. Such ring alignment specs have already been achieved more than ten years ago [30, 31] by mechanical means using water levels.

E. General Relativity

Since we live in relativity, general relativistic effects caused by the gravity and rotation of the Earth can manifest themselves in some high-precision experiments. The spin dynamics in the considered pEDM experiment is also affected by such effects. In connection with the Equivalence Principle, one can always introduce a *local* Lorentz (anholonomic) coordinate system based on a tetrad of appropriate orthogonal coordinate vectors. Dynamics of the momentum and spin in this coordinate system is defined by equations of motion formally coinciding with usual equations given by electrodynamics in the Minkowski spacetime [32–34]. The general relativistic effects in storage ring EDM experiments have been analyzed in previous studies [34–38] and the corresponding systematic corrections have been calculated. It has been explicitly shown in Refs. [38] that the final results obtained in these studies perfectly agree with each other.

F. Spin coherence time

The Spin Coherence Time (SCT), also known as in plane polarization (IPP) lifetime, preservation during

storage is essential to achieve the desired sensitivity requirements [20]. EDM search with longitudinally polarized beam requires SCT of around 1000 s. It has been shown that long SCTs are correlated with zero chromaticity conditions [39, 40], which are defined as,

$$\xi_{x,y} = \frac{\delta Q_{x,y}/Q_{x,y}}{\delta p/p}.$$

Sextupole fields compensate for chromaticity and hence a much increased SCT as it recently has been experimentally shown at COSY [41].

We want to demonstrate a long SCT by using magnetic sextupoles defined as,

$$\begin{aligned} B_x &= 2k^m xy \\ B_y &= k^m(x^2 - y^2). \end{aligned}$$

We put the magnetic sextupole pair k_1^m, k_2^m on top of the magnetic quadrupoles (Figure 1) in order not to break the symmetric conditions of the lattice. We show that a single particle precession rate can be significantly improved if the correct sextupole fields are used — Figure 11. We empirically found that optimum sextupole pair strength for a single non-reference particle is very close to the optimum for a particle bunch.

Nevertheless, the sextupoles could have been electric instead,

$$\begin{aligned} E_y &= -2k^e xy \\ E_x &= k^e(x^2 - y^2), \end{aligned}$$

and we observe similar spin precession behavior — Figure 12.

However, as the optimal pair (electric or magnetic) of sextupole strengths $k_1^{m,e}, k_2^{m,e}$ (Figures 11 and 12) is not symmetric w.r.t. CW-CCW beams, the SCT could be improved in one beam direction only. We can get away with this solution if we allow the beams to be injected at separately and adjust the sextupole strengths accordingly for each beam direction.

Alternatively, this can be solved by incorporating magnetic and electric sextupoles at the same time. Symmetry of the problem (Figures 11 and 12) shows that CW and CCW beams experience the same effect from magnetic and electric sextupoles if,

$$\begin{aligned} k^m &= k_1^m = -k_2^m \\ k^e &= k_1^e = k_2^e, \end{aligned} \tag{6}$$

Hence, having both magnetic and electric sextupoles that obey Equation (6) will lead to a better SCT for both CW and CCW beams — Figure 13. By incorporating the best pair k^m, k^e we see that the SCT improves vastly for both CW and CCW beams at the same time — Figure 14. Additional details about finding the optimum sextupole strengths is given in Appendix B.

G. Polarimeter systematic issues

A prototype polarimeter for the EDM ring has been constructed and commissioned [42] with 0.97 GeV/c polarized deuterons at the COSY storage ring located at the Forschungszentrum Jülich. A cross-sectional view of the main parts is shown in Figure 10

The polarimeter is sensitive to forward-going elastically-scattered particles in the angle range between 4° and 15° . The acceptance is defined by the LYSO crystals, which are grouped according to the direction of scatter as left (L), up (U), right (R), and down (D).

The polarimeter is most sensitive to deviations of the beam from the central polarimeter axis. For forward-angle polarimeters, position and angle errors create similar effects and may be grouped together for remediation. Most first-order errors may be eliminated by comparing count rates taken with the polarization pointing forward (+) and backward (-) as,

$$\bar{p} = \frac{2}{3A} \frac{r-1}{r+1} \quad r^2 = \frac{L_+ R_-}{L_- R_+}$$

where A is analyzing power of the polarimeter.

But accurately measuring small polarization rotations at the level of μrad means being able to handle errors beyond first order. To do this, we must create a model of the terms driving these errors provide a means of making corrections for them in real time if possible. Such a model was created for the original polarimeter used in beam studies at COSY [43]. There must also be parameters that scale the corrections that are themselves sensitive in first order to the driving terms. One such choice is,

$$\phi = \frac{s-1}{s+1} \quad s^2 = \frac{L_+ R_+}{L_- R_-}$$

which is sensitive to geometric errors in first order but not to the polarization and

$$W = \frac{dL_+}{dt} + \frac{dR_+}{dt} + \frac{dR_-}{dt} + \frac{dL_-}{dt}$$

which is sensitive to the sum of the detector count rates for correcting rate-dependent errors. Next a calibration must be performed of the sensitivity of the polarimeter to various orders of angle/position errors as a function of these two driving terms. Once in place, monitoring the size of these two terms allows a correction to be made to any polarization observable in real time. This was tested at COSY and proved correct to a level of 10^{-5} (limited by statistics) with no suggestion that the method was encountering a limit.

There are a number of systematic effects that rely on the comparison of asymmetries measured with counter-rotating beams (CW and CCW). Most likely, this will mean two sets of forward detectors mounted on either side of a single target that is shared by the two beams.

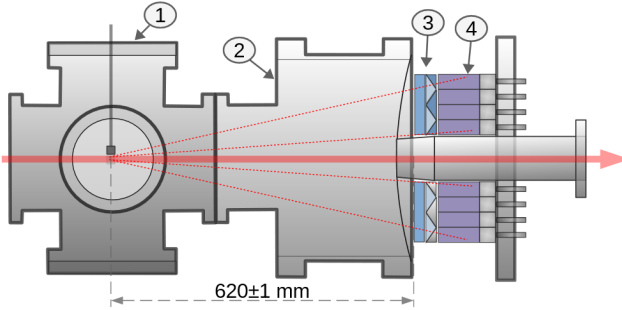


FIG. 10. Prototype EDM polarimeter showing (1) target chamber with 2-cm thick carbon block target located at the edge of the beam, (2) expansion chamber for scattered particles with an 800 μm thick stainless steel exit window, (3) double layer ΔE scintillation detector for position tracking, and (4) 8-cm deep LYSO crystal calorimeter. The detector is read out through SiPM wafers.

For elastic scattering from carbon, backscattering from the target is usually less than 10^{-7} of the forward scattering rate and should not be an issue. But the two polarimeters will be separate instruments, and the calibration of their response to polarization must be precise enough that the difference of the asymmetries they yield is meaningful at the level of 10^{-6} , what is needed for the EDM search.

IV. DISCUSSION AND CONCLUSION

A. Simulation with realistic conditions

We demonstrate the feasibility of the experiment, by incorporating multiple lattice imperfections, such as both horizontal and vertical quadrupole misalignment and deflector tilts. All in all, we require the CW-CCW beams to vertically overlap within $\pm 5 \mu\text{m}$ with $\pm 50 \mu\text{m}$ overall vertical closed orbit planarity. With such conditions, we first numerically verify that the established realistic conditions are met – Figure 15. Later, vertical magnetic field B_y and RF cavity frequency is adjusted until no discernible (less than $\sim 1 \mu\text{rad/s}$) unwanted radial precession is present. Adjusting is needed as the closed orbit changes due to various lattice misalignments. Lastly, we run with both normal and reversed magnetic quadrupole polarities and look at the total EDM signal which should be calculated as in Equation (3).

Upon examining the result – Figure 16, we conclude that the unwanted background residual EDM-like signal is below target experimental sensitivity; hence, we verify that the systematic error sources with such lattice alignment requirements are low enough to allow the measuring proton electric dipole moment to $d = 10^{-29} e\cdot\text{cm}$.

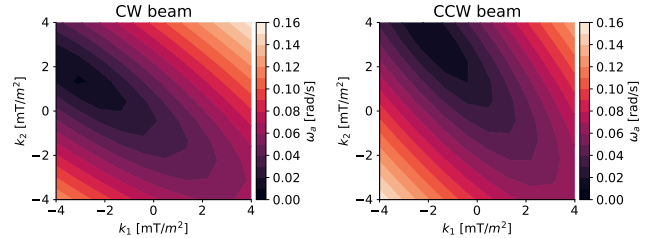


FIG. 11. Single particle horizontal precession rate ω_a as a function of magnetic sextupole strengths k_1, k_2 . Darker — lower ω_a ; thus, better SCT. Left: CW beam, right: CCW beam. The axis of the symmetry is $k_1 = -k_2$, hence the apparent transposition w.r.t. CW-CCW beams.

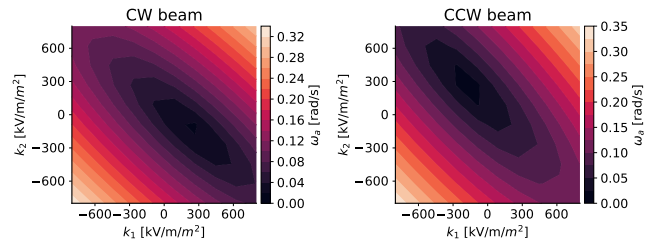


FIG. 12. Single particle horizontal precession rate ω_a as a function of electric sextupole strengths k_1, k_2 . Darker — lower ω_a ; thus, better SCT. Left: CW beam, right: CCW beam. The axis of the symmetry is $k_1 = +k_2$, hence the apparent transposition w.r.t. CW-CCW beams.

B. Spin-based alignment

Spin-based alignment (SBA) is inspired by the ideas of the Beam-based alignment (BBA) and serves as a more sensitive, spin-based beam monitoring tool. Spin-measurements have been proven to be extremely sensitive to electromagnetic fields, as it has seen many times in practice [7–10]. We propose to use spin measurements as feedback for ring alignment purposes. As it was shown here, spin is very sensitive to various lattice imperfections; hence, spin information could be used as a probe

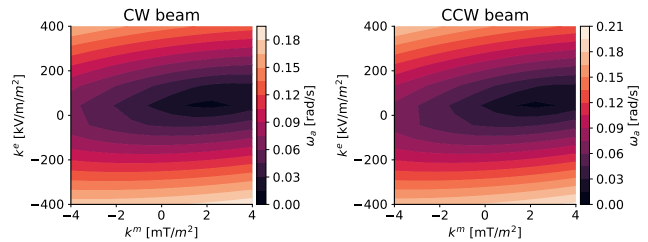


FIG. 13. Single particle horizontal precession rate ω_a as a function of magnetic and electric sextupole strengths k^m, k^e (Equation (6)). Darker — lower ω_a ; thus, better SCT. Left: CW beam, right: CCW beam. The effect is perfectly symmetric as the variables can only affect CW-CCW beams the same way. Thus, we can improve the SCT for both cases at the same time.

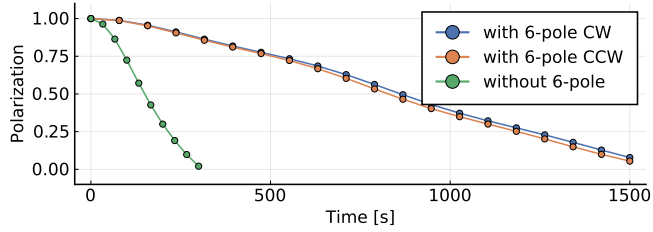


FIG. 14. Magnitude of the polarization vector vs. time simulation with a realistic bunch structure given as, $\Delta x/x = \pm 4\text{ mm}$, $\Delta y/y = \pm 3\text{ mm}$. The polarization retains a high value with hybrid (magnetic and electric) sextupoles for both CW (blue) and CCW (orange) bunches compared to the nominal case without sextupoles (green). The simulation is sub-second long, with the polarization at $t \gg 1\text{ s}$ estimated by measuring precession rate for each particle, then extrapolated with corresponding error propagation.

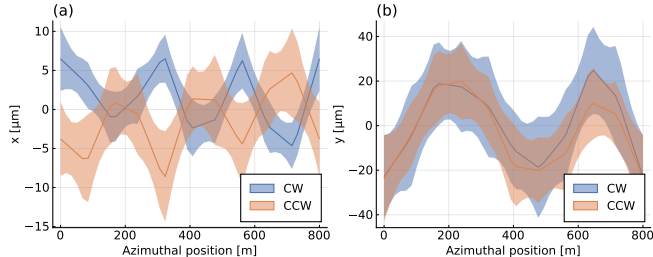


FIG. 15. Single particle position averaged over 5×10^5 turns at split onto 48 bins. (a) Horizontal position throughout the ring azimuth. (b) Vertical position throughout the ring azimuth. Fill color shows standard deviations at the bins, roughly giving the idea about the spread.

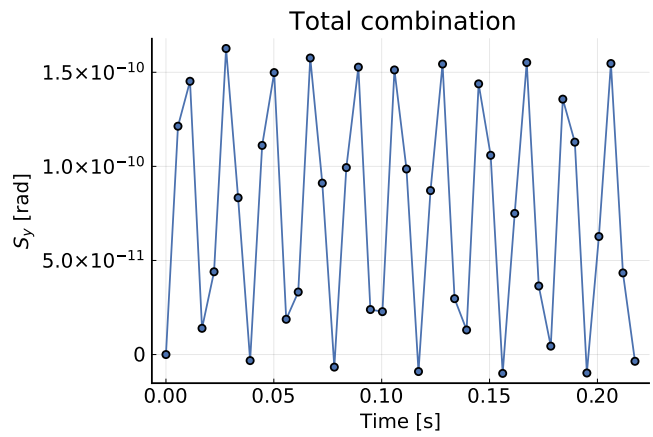


FIG. 16. Vertical spin component S_y vs. storage time. The signal comes from calculation of Equation (3), with residual EDM-mimicking background precession rate of $dS_y/dt < 1\text{ nrad/s}$ which corresponds to the target sensitivity of $d = 10^{-29}\text{ e}\cdot\text{cm}$. The actual numerical vertical spin data oscillates rapidly; hence it was arbitrarily averaged onto 40 points.

to further align storage ring elements.

For instance, for the storage ring proton EDM experiment, if additional sensitivity would ever be required, radially polarized beams could be used to investigate vertical velocity systematic (Section III A), as the effect of the systematic is maximal with radially polarized beams. Further, SBA could be used to further investigate Geometrical phase, Spin coherence times issues too.

In general, SBA is not restricted to having a radial polarization direction as a feedback system for leveling the ring elements. Other systematics or ring alignment issues could be addressed using radial, longitudinal and/or vertical spin directions.

C. Conclusions

The most important systematic error issues in the storage ring proton EDM experiment are covered. This paper has introduced novel methods of improving the sensitivity of the experiment such as Symmetric Ring design and Spin-based alignment, and demonstrated the ring alignment requirements.

D. Acknowledgments

This work was supported by IBS-R017-D1-2020-a00.

Appendix A: High precision tracking

Lorentz equation governs dynamics of a particle in EM fields,

$$\frac{d\vec{\beta}}{dt} = \frac{e}{m\gamma c} \left[\vec{E} + c\vec{\beta} \times \vec{B} - \beta(\vec{\beta} \cdot \vec{E}) \right].$$

However, its perturbative expansion in particle optical coordinates is more practical for storage rings and accelerators, as we are using natural variables of interest [44],

$$\begin{aligned} x' &= a(1 + hx) \frac{p_0}{p_s} \\ a' &= (1 + hx) \left[\frac{1 + \eta}{1 + \eta_0} \frac{E_x}{\chi_{e0}} \frac{p_0}{p_s} + b \frac{B_s}{\chi_{m0}} \frac{p_0}{p_s} - \frac{B_y}{\chi_{m0}} \right] + h \frac{p_s}{p_0} \\ y' &= b(1 + hx) \frac{p_0}{p_s} \\ b' &= (1 + hx) \left[\frac{1 + \eta}{1 + \eta_0} \frac{E_y}{\chi_{e0}} \frac{p_0}{p_s} + \frac{B_x}{\chi_{m0}} - a \frac{B_s}{\chi_{m0}} \frac{p_0}{p_s} \right], \end{aligned}$$

where prime indicates differentiation with respect to s beamline travel distance, subscript 0 is the quantity w.r.t. the reference particle. In this curvilinear (Frenet-Serret) coordinate system, x indicates radial deviation from the reference orbit, y indicates vertical deviation,

and s points along the direction of motion of the reference particle. Hence, the momentum in this coordinate system is measured in $\vec{p}/p_0 = (a, b, p_s/p_0)$. Other variables, $h = 1/R_0$ indicates curvature for the reference orbit, $\chi_{e0}, \chi_{m0} = p_0 v/Ze, p_0/Ze$ electric and magnetic rigidities, $\eta = \gamma - 1$ the relativistic measure.

The spin vector should be integrated with BMT equation [45, 46], given in Cartesian coordinates as follows,

$$\frac{d\vec{S}}{dt} = \vec{\Omega} \times \vec{S}$$

$$\begin{aligned} \frac{d\vec{S}}{dt} = \frac{e}{m} \vec{S} \times & \left[\left(a + \frac{1}{\gamma} \right) \vec{B} - \frac{a\gamma}{\gamma+1} \vec{\beta} (\vec{\beta} \cdot \vec{B}) \right. \\ & \left. - \left(a + \frac{1}{\gamma+1} \right) \frac{\vec{\beta} \times \vec{E}}{c} \right. \quad (\text{A1}) \\ & \left. + \frac{\eta}{2} \left(\frac{\vec{E}}{c} - \frac{\gamma}{\gamma+1} \frac{\vec{\beta}}{c} (\vec{\beta} \cdot \vec{E}) + \vec{\beta} \times \vec{B} \right) \right]. \end{aligned}$$

However, as we would like the normalized to unity spin vector measured in terms of $\vec{S} = (S_x, S_y, S_z)$ — radial, vertical, and longitudinal spin components, the original BMT equation (Equation (A1)) needs to be modified as,

$$\vec{S}' = \left(\vec{\Omega} t' - \hat{y}/h \right) \times \vec{S},$$

in order to compensate for the rotation of the coordinate system itself, and take into account that we want the derivative w.r.t. s integration variable.

Each of the storage ring elements have been tracked separately in order to avoid discontinuities in EM fields that directly lead to unstable numerical integration. Electric bending plates were hard-edge approximated. The fields inside cylindrical deflectors with a focusing index $n = m + 1$ are given as [47, 48],

$$\begin{aligned} E_x &= -E_0 \left(1 - \frac{nx}{R_0} + \frac{n(n+1)x^2}{2R_0^2} \right) \\ E_y &= -E_0 \left((n-1) \frac{y}{R_0} \right). \end{aligned}$$

It is important to note that in order to meet the precision requirements, second order terms (x^2) must be considered to have precise spin integration.

Appendix B: Optimum sextupole search

As we have seen on Figures 11 to 13 the optimal sextupole strengths pair is obtained first by a rough 2-dimensional parameter sweep, followed by numerical optimization to find the finer minimum. Additionally, finding optimal pairs for magnetic and electric sextupoles separately is sufficient to infer the value for the optimum strength needed for hybrid sextupoles.

Let us suppose that $k_1^m = \alpha_1, k_2^m = -\beta_1$ is the optimal pair for magnetic sextupoles for CW beam, with $k_1^m = \beta_1, k_2^m = -\alpha_1$ for the CCW case. Similarly, $k_1^e = -\alpha_2, k_2^e = \beta_2$ and $k_1^e = \beta_2, k_2^e = -\alpha_2$ for CW and CCW directions respectively with electric sextupoles.

By observing the symmetry in Figures 11 and 12, we can infer that,

$$k_1^m = -\frac{\alpha_1}{\alpha_2} \times k_1^e \quad k_2^m = -\frac{\beta_1}{\beta_2} \times k_2^e \quad \text{for CW} \quad (\text{B1})$$

$$k_1^m = \frac{\beta_1}{\beta_2} \times k_1^e \quad k_2^m = \frac{\alpha_1}{\alpha_2} \times k_2^e \quad \text{for CCW} \quad (\text{B2})$$

i.e. only a sign change is required for transition from electric to magnetic or vice versa. We can also infer the conversion factor from electric to magnetic sextupoles. Following the lines of the symmetry, we can find the optimal pair for hybrid sextupoles case in magnetic units,

$$M_1 + E_1 = \alpha_1 \quad -M_1 + E_1 = -\beta_1 \quad (\text{B3})$$

solving for each $M_1 = (\alpha_1 + \beta_1)/2$ and $E_1 = \alpha_2/\alpha_1 \times (\alpha_1 - \beta_1)/2$ we get the optimal pair for each case in proper units. Figures 11 to 13 verify these analytical estimations to 1% accuracy.

[1] E. M. Purcell and N. F. Ramsey, On the possibility of electric dipole moments for elementary particles and nuclei, *Physical Review* **78**, 807.

[2] L. Landau, On the conservation laws for weak interactions, *Nuclear Physics* **3**, 127.

[3] J. M. Pendlebury, S. Afach, N. J. Ayres, C. A. Baker, G. Ban, G. Bison, K. Bodek, M. Burghoff, P. Geltenbort, K. Green, W. C. Griffith, M. van der Grinten, Z. D. Grujić, P. G. Harris, V. Hélaïne, P. Iaydjiev, S. N. Ivanov, M. Kasprzak, Y. Kermaidic, K. Kirch, H.-C. Koch,

S. Komposch, A. Kozela, J. Krempel, B. Lauss, T. Lefort, Y. Lemièvre, D. J. R. May, M. Musgrave, O. Naviliat-Cuncic, F. M. Piegsa, G. Pignol, P. N. Prashanth, G. Quéméner, M. Rawlik, D. Rebreyend, J. D. Richardson, D. Ries, S. Roccia, D. Rozpedzik, A. Schnabel, P. Schmidt-Wellenburg, N. Severijns, D. Shiers, J. A. Thorne, A. Weis, O. J. Winston, E. Wursten, J. Zejma, and G. Zsigmond, Revised experimental upper limit on the electric dipole moment of the neutron, *Phys. Rev. D* **92**, 092003 (2015).

[4] V. Andreev, D. G. Ang, D. DeMille, J. M. Doyle, G. Gabrielse, J. Haefner, N. R. Hutzler, Z. Lasner, C. Meisenhelder, B. R. O'Leary, C. D. Panda, A. D. West, E. P. West, X. Wu, and ACME Collaboration, Improved limit on the electric dipole moment of the electron, *Nature* **562**, 355, number: 7727 Publisher: Nature Publishing Group.

[5] J. Baron, W. C. Campbell, D. DeMille, J. M. Doyle, G. Gabrielse, Y. V. Gurevich, P. W. Hess, N. R. Hutzler, E. Kirilov, I. Kozyryev, B. R. O'Leary, C. D. Panda, M. F. Parsons, E. S. Petrik, B. Spaun, A. C. Vutha, and A. D. West, Order of magnitude smaller limit on the electric dipole moment of the electron, *Science* **343**, 269, publisher: American Association for the Advancement of Science eprint: <https://science.scienmag.org/content/343/6168/269.full.pdf>.

[6] B. Graner, Y. Chen, E. G. Lindahl, and B. R. Heckel, Reduced limit on the permanent electric dipole moment of ^{199}Hg , *Phys. Rev. Lett.* **116**, 161601 (2016).

[7] G. Charpak, F. Farley, R. L. Garwin, T. Muller, J. C. Sens, and A. Zichichi, A new measurement of the anomalous magnetic moment of the muon, *Phys. Letters* **1** (1962).

[8] J. Bailey, W. Bartl, G. von Bochmann, R. Brown, F. Farley, M. Giesch, H. Jöstlein, S. Van der Meer, E. Picasso, and R. Williams, Precise measurement of the anomalous magnetic moment of the muon, *Il Nuovo Cimento A (1965-1970)* **9**, 369 (1972).

[9] J. Bailey, K. Borer, F. Combley, H. Drumm, C. Eck, F. Farley, J. Field, W. Flegel, P. Hattersley, F. Krienen, *et al.*, Final report on the cern muon storage ring including the anomalous magnetic moment and the electric dipole moment of the muon, and a direct test of relativistic time dilation, *Nuclear Physics B* **150**, 1 (1979).

[10] G. W. Bennett, B. Bousquet, H. N. Brown, G. Bunce, R. M. Carey, P. Cushman, G. T. Danby, P. T. Debevec, M. Deile, H. Deng, W. Deninger, S. K. Dhawan, V. P. Druzhinin, L. Duong, E. Efstathiadis, F. J. M. Farley, G. V. Fedotovich, S. Giron, F. E. Gray, D. Grigoriev, M. Grosse-Perdekamp, A. Grossmann, M. F. Hare, D. W. Hertzog, X. Huang, V. W. Hughes, M. Iwasaki, K. Jungmann, D. Kawall, M. Kawamura, B. I. Khazin, J. Kindem, F. Krienen, I. Kronqvist, A. Lam, R. Larsen, Y. Y. Lee, I. Logashenko, R. McNabb, W. Meng, J. Mi, J. P. Miller, Y. Mizumachi, W. M. Morse, D. Nikas, C. J. G. Onderwater, Y. Orlov, C. S. Özben, J. M. Parley, Q. Peng, C. C. Polly, J. Pretz, R. Prigl, G. zu Putlitz, T. Qian, S. I. Redin, O. Rind, B. L. Roberts, N. Ryskulov, S. Sedykh, Y. K. Semertzidis, P. Shagin, Y. M. Shatunov, E. P. Sichtermann, E. Solodov, M. Sossong, A. Steinmetz, L. R. Sulak, C. Timmermans, A. Trofimov, D. Urner, P. von Walter, D. Warburton, D. Winn, A. Yamamoto, and D. Zimmerman, Final report of the e821 muon anomalous magnetic moment measurement at BNL, *Physical Review D* **73**, 10.1103/PhysRevD.73.072003.

[11] V. Anastassopoulos, S. Andrianov, R. Baartman, S. Baessler, M. Bai, J. Benante, M. Berz, M. Blaskiewicz, T. Bowcock, K. Brown, B. Casey, M. Conte, J. D. Crnkovic, N. D'Imperio, G. Fanourakis, A. Fedotov, P. Fierlinger, W. Fischer, M. O. Gaisser, Y. Giomataris, M. Grosse-Perdekamp, G. Guidoboni, S. Haciomeroglu, G. Hoffstaetter, H. Huang, M. Incagli, A. Ivanov, D. Kawall, Y. I. Kim, B. King, I. A. Koop, D. M. Lazarus, V. Lebedev, M. J. Lee, S. Lee, Y. H. Lee, A. Lehrach, P. Lenisa, P. L. Sandri, A. U. Luccio, A. Lyapin, W. MacKay, R. Maier, K. Makino, N. Malitsky, W. J. Marciano, W. Meng, F. Meot, E. M. Metodiev, L. Miceli, D. Moricciani, W. M. Morse, S. Nagaitsev, S. K. Nayak, Y. F. Orlov, C. S. Ozben, S. T. Park, A. Pesce, E. Petrakou, P. Pile, B. Podobedov, V. Polychronakos, J. Pretz, V. Ptitsyn, E. Ramberg, D. Raparia, F. Rathmann, S. Rescia, T. Roser, H. K. Sayed, Y. K. Semertzidis, Y. Senichev, A. Sidorin, A. Silenko, N. Simos, A. Stahl, E. J. Stephenson, H. Ströher, M. J. Syphers, J. Talman, R. M. Talman, V. Tishchenko, C. Touramanis, N. Tsoupas, G. Venanzoni, K. Vetter, S. Vlassis, E. Won, G. Zavattini, A. Zelenski, and K. Zioutas, A storage ring experiment to detect a proton electric dipole moment, *Review of Scientific Instruments* **87**, 115116 () .

[12] S. Haciomeroglu, Y. F. Orlov, and Y. K. Semertzidis, Magnetic field effects on the proton EDM in a continuous all-electric storage ring, *Nuclear Instruments and Methods in Physics Research Section A: Accelerators, Spectrometers, Detectors and Associated Equipment* **927**, 262.

[13] S. Haciomeroglu and Y. K. Semertzidis, A hybrid ring design in the storage-ring proton electric dipole moment experiment, *arXiv:1806.09319 [physics]* 1806.09319.

[14] V. Bargmann, L. Michel, and V. L. Telegdi, Precession of the polarization of particles moving in a homogeneous electromagnetic field, *Phys. Rev. Lett.* **2**, 435 (1959).

[15] T. FUKUYAMA and A. J. SILENKO, Derivation of generalized thomas-bargmann-michel-telegdi equation for a particle with electric dipole moment, *International Journal of Modern Physics A* **28**, 1350147 (2013), <https://doi.org/10.1142/S0217751X13501479>.

[16] I. B. Khriplovich, Feasibility of search for nuclear electric dipole moments at ion storage rings, *Physics Letters B* **444**, 98 .

[17] A. J. Silenko, Equation of spin motion in storage rings in the cylindrical coordinate system, *Physical Review Special Topics-Accelerators and Beams* **9**, 034003 (2006).

[18] S. Mane, Orbital dynamics in a storage ring with electrostatic bending, *Nuclear Instruments and Methods in Physics Research Section A: Accelerators, Spectrometers, Detectors and Associated Equipment* **596**, 288 () .

[19] S. Mane, Orbital and spin motion in a storage ring with static electric and magnetic fields, *Nuclear Instruments and Methods in Physics Research Section A: Accelerators, Spectrometers, Detectors and Associated Equipment* **687**, 40 () .

[20] V. Anastassopoulos *et al.*, A proposal to measure the proton electric dipole moment with $10^{-29}e\cdot\text{cm}$ sensitivity, by the Storage ring EDM collaboration <http://www.bnl.gov/edm> () .

[21] F. J. M. Farley, K. Jungmann, J. P. Miller, W. M. Morse, Y. F. Orlov, B. L. Roberts, Y. K. Semertzidis, A. Silenko, and E. J. Stephenson, New method of measuring electric dipole moments in storage rings, *Physical Review Letters* **93**, 052001.

[22] C. Tsitouras, Runge-kutta pairs of order 5(4) satisfying only the first column simplifying assumption, *Computers & Mathematics with Applications* **62**, 770.

[23] P. Tenenbaum and T. Raubenheimer, Resolution and systematic limitations in beam-based alignment, *Physical Review Special Topics-Accelerators and Beams* **3**, 052801 (2000).

[24] S. Haciomeroglu, D. Kawall, Y.-H. Lee, A. Matlashov, Z. Omarov, and Y. K. Semertzidis, Squid-based beam position monitor, The 39th International Conference on High Energy Physics, ICHEP2018 (2018).

[25] S. Haciomeroglu, to be published, .

[26] M. V. Berry, Quantal Phase Factors Accompanying Adiabatic Changes, Proceedings of the Royal Society of London Series A **392**, 45 (1984).

[27] C. A. Baker, D. D. Doyle, P. Geltenbort, K. Green, M. G. D. van der Grinten, P. G. Harris, P. Iaydjiev, S. N. Ivanov, D. J. R. May, J. M. Pendlebury, J. D. Richardson, D. Shiers, and K. F. Smith, Improved experimental limit on the electric dipole moment of the neutron, Phys. Rev. Lett. **97**, 131801 (2006).

[28] J. M. Pendlebury, W. Heil, Y. Sobolev, P. G. Harris, J. D. Richardson, R. J. Baskin, D. D. Doyle, P. Geltenbort, K. Green, M. G. D. van der Grinten, P. S. Iaydjiev, S. N. Ivanov, D. J. R. May, and K. F. Smith, Geometric-phase-induced false electric dipole moment signals for particles in traps, Phys. Rev. A **70**, 032102 (2004).

[29] A. J. Silenko, Berry phases in an electric-dipole-moment experiment in an all-electric storage ring, arXiv:1710.01609 [hep-ex, physics:hep-th, physics:nucl-ex, physics:physics] 1710.01609.

[30] B. Yang and H. Friedsam, High-resolution accelerator alignment using x-ray optics, Physical Review Special Topics - Accelerators and Beams **9**, 030701, publisher: American Physical Society.

[31] V. Shiltsev, Space-time diffusion of ground and its fractal nature, , 83.

[32] A. J. Silenko, Local lorentz transformations and thomas effect in general relativity, Phys. Rev. D **93**, 124050 (2016).

[33] Y. N. Obukhov, A. J. Silenko, and O. V. Teryaev, Manifestations of the rotation and gravity of the earth in high-energy physics experiments, Phys. Rev. D **94**, 044019 (2016).

[34] Y. N. Obukhov, A. J. Silenko, and O. V. Teryaev, General treatment of quantum and classical spinning particles in external fields, Phys. Rev. D **96**, 105005 (2017).

[35] A. J. Silenko and O. V. Teryaev, Equivalence principle and experimental tests of gravitational spin effects, Phys. Rev. D **76**, 061101 (2007).

[36] Y. Orlov, E. Flanagan, and Y. Semertzidis, Spin rotation by earth's gravitational field in a frozen-spin ring, Physics Letters A **376**, 2822 (2012).

[37] A. László and Z. Zimborás, Quantification of gr effects in muon g-2, edm and other spin precession experiments, Classical and Quantum Gravity **35**, 175003 (2018).

[38] S. Vergeles and N. Nikolaev, Gravitational effects in electrostatic storage rings and the search for the electric dipole moments of charged particles, Journal of Experimental and Theoretical Physics **129**, 541 (2019).

[39] I. B. Vasserman, P. V. Vorobyov, E. S. Gluskin, P. M. Ivanov, I. A. Koop, G. Y. Kezerashvili, A. P. Lysenko, I. N. Nesterenko, E. A. Perevedentsev, A. A. Mikhailichenko, A. A. Polunin, S. I. Serednyakov, A. N. Skrinsky, and Y. M. Shatunov, Comparison of the electron and positron anomalous magnetic moments: Experiment 1987, Physics Letters B **198**, 302.

[40] I. Koop and J. M. Shatunov, The spin precession tune spread in the storage ring, in *European particle accelerator conference* (1988).

[41] JEDI Collaboration, G. Guidoboni, E. Stephenson, S. Andrianov, W. Augustyniak, Z. Bagdasarian, M. Bai, M. Baylac, W. Bernreuther, S. Bertelli, M. Berz, J. Böker, C. Böhme, J. Bsaisou, S. Chekmenev, D. Chiladze, G. Ciullo, M. Contalbrigo, J.-M. de Conto, S. Dymov, R. Engels, F. Esser, D. Eversmann, O. Felden, M. Gaisser, R. Gebel, H. Glückler, F. Goldenbaum, K. Grigoryev, D. Grzonka, T. Hahnrats, D. Heberling, V. Hejny, N. Hempelmann, J. Hetzel, F. Hinder, R. Hippel, D. Hölscher, A. Ivanov, A. Kacharava, V. Kamerdzhev, B. Kamys, I. Keshelashvili, A. Khokhlov, I. Koop, H.-J. Krause, S. Krewald, A. Kulikov, A. Lehrach, P. Lenisa, N. Lomidze, B. Lorentz, P. Maanen, G. Macharashvili, A. Magiera, R. Maier, K. Makino, B. Mariański, D. Mchedlishvili, U.-G. Meißner, S. Mey, W. Morse, F. Müller, A. Nass, G. Natour, N. Nikolaev, M. Nioradze, K. Nowakowski, Y. Orlov, A. Pesce, D. Prasuhn, J. Pretz, F. Rathmann, J. Ritman, M. Rosenthal, Z. Rudy, A. Saleev, T. Sefzick, Y. Semertzidis, Y. Senichev, V. Shmakova, A. Silenko, M. Simon, J. Slim, H. Soltner, A. Stahl, R. Stassen, M. Statera, H. Stockhorst, H. Straatmann, H. Ströher, M. Tabidze, R. Talman, P. Thörngren Engblom, F. Trinkel, A. Trzciński, Y. Uzikov, Y. Valdau, E. Valetov, A. Vassiliev, C. Weidemann, C. Wilkin, A. Wrońska, P. Wüstner, M. Zakrzewska, P. Zuprański, and D. Zyuzin, How to reach a thousand-second in-plane polarization lifetime with $\$0.97\text{ GeV}/c^2$ deuterons in a storage ring, Physical Review Letters **117**, 054801, publisher: American Physical Society.

[42] F. Müller, O. Javakhishvili, D. Shergelashvili, I. Keshelashvili, D. Mchedlishvili, F. Abusaif, A. Aggarwal, L. Barion, S. Basile, J. Böker, et al., A new beam polarimeter at cosy to search for electric dipole moments of charged particles, Journal of Instrumentation **15** (12), P12005.

[43] N. Brantjes, V. Dzordzhadze, R. Gebel, F. Gonnella, F. Gray, D. Van der Hoek, A. Imig, W. Kruithof, D. Lazarus, A. Lehrach, et al., Correcting systematic errors in high-sensitivity deuteron polarization measurements, Nuclear Instruments and Methods in Physics Research Section A: Accelerators, Spectrometers, Detectors and Associated Equipment **664**, 49 (2012).

[44] M. Berz, *An Introduction to Beam Physics*, 1st ed. (CRC Press).

[45] V. Bargmann, L. Michel, and V. L. Telegdi, Precession of the polarization of particles moving in a homogeneous electromagnetic field, Phys. Rev. Lett. **2**, 435 (1959).

[46] T. FUKUYAMA and A. J. SILENKO, Derivation of generalized thomas-bargmann-michel-telegdi equation for a particle with electric dipole moment, International Journal of Modern Physics A **28**, 1350147 (2013), <https://doi.org/10.1142/S0217751X13501479>.

[47] E. Metodiev, K. Huang, Y. Semertzidis, and W. Morse, Fringe electric fields of flat and cylindrical deflectors in electrostatic charged particle storage rings, Physical Review Special Topics - Accelerators and Beams **17**, 074002 (), publisher: American Physical Society.

[48] E. Metodiev, I. D'Silva, M. Fandarov, M. Gaisser, S. Haciomeroglu, D. Huang, K. Huang, A. Patil, R. Prodromou, O. Semertzidis, D. Sharma, A. Stamatakis, Y. Orlov, and Y. Semertzidis, Analytical benchmarks for precision particle tracking in electric and magnetic rings, Nuclear Instruments and Methods in Physics Research

Section A: Accelerators, Spectrometers, Detectors and
Associated Equipment **797**, 311 ()�